RESEARCH PAPERS

Direct Inversion of Dynamical Electron Diffraction Patterns to Structure Factors

J. C. H. SPENCE

Department of Physics, Arizona State University, Tempe, AZ 85287, USA. E-mail: spence@asu.edu

Abstract

An exact nonperturbative inversion method is described for transmission electron diffraction which allows crystal structure factors to be obtained directly from the intensities of multiply scattered Bragg beams. These amplitudes are required at several thicknesses (or electron beam energies) and orientations of a thin crystal. The analysis applies to centrosymmetric crystals with anomalous absorption and to noncentrosymmetric crystals if the mean absorption potential only is included. Phases of stucture factors from noncentrosymmetric crystals are correctly recovered. Dynamical coherent convergent-beam microdiffraction patterns with overlap of adjacent diffraction orders, provide the required data and may be obtained from nanometer-sized regions. The method allows the direct synthesis of charge-density maps of unknown crystal structures at high resolution from electron microdiffraction patterns, using a scanning transmission electron microscope. Whereas this microscope must be capable of resolving only the first-order lattice spacing, much higher order reflections may in principle be determined. Such a charge-density map provides fractional atomic coordinates and the identification of atomic species (as in X-ray crystallography) from microcrystalline samples and other multiphase inorganic materials for which large single crystals cannot be obtained or X-ray powder patterns obtained or analyzed. In other language, this paper solves the inversion problem of quantum mechanics for the case of electron scattering from a periodic potential, described by the Schroedinger equation, in which the scattering is given as a function of some parameter and the potential sought. The diagonalization of large matrices is required – the method does not provide a closed-form solution.

1. Introduction

The measurement of crystal structure factors by electron diffraction has a long history (Cowley, 1978, 1992). By comparison with X-ray diffraction, the simultaneous excitation of hundreds of Bragg reflections is common in transmission electron diffraction, a consequence of the very large Ewald-sphere radius. To date, the most sucessful structure-refinement methods have been those that assume single-scattering conditions and combine diffraction and high-resolution imaging data (see Dorset, 1995, for a review). They are therefore limited to thin films less than a few nanometers in thickness and are ideally suited to the study of organic membranes or two-dimensional crystals. For small-unit-cell inorganic crystals of known structure, several methods of structure-factor measurement exist, including the intersecting Kikuchi-line method (Gjønnes & Høier, 1971) and the critical-voltage method (Uyeda, 1968), both closely related to the Renninger effect of X-ray diffraction. These are useful for the study of bond charge densities. More recently, both amplitude and phase measurements of structure factors have been made with high accuracy by automated adjustment of forward dynamical computations for agreement with convergent-beam rocking curves. In this way, for example, structure-factor phases have been obtained from noncentrosymmetric (acentric) crystals with an accuracy of better than one tenth of a degree (Zuo, Spence, Downs & Mayer, 1993), greatly exceeding the accuracy possible using X-ray diffraction and so allowing the study of bonding in noncentrosymmetric crystals. The extension of these multiple-scattering optimization methods to the refinement of atomic positions is under way in several laboratories. Alternatively, approximations to the dynamical equations that emphasize the dominant bound transverse eigenstates may be used to determine unknown structures in combination with conditional Patterson functions (Vincent, Bird & Steeds, 1984). Most recently, an inversion scheme has been proposed based on high-resolution electron holograms (Scheerschmidt & Knoll, 1995).

The direct inversion of multiple-scattering electron diffraction patterns has challenged theoreticians for many years. The multislice theory of electron diffraction, for example, was developed for the purposes of finding a closed-form inversion and computational inversion algorithms continue to be developed based on this method (Spargo, Beeching & Allen, 1994). Since a closed-form Bloch-wave solution has been given for the general three-beam case (Kambe, 1957), there has been great interest in cases reducible to this solution. For centrosymmetric

crystals, this has recently been shown by elegant methods to be invertible (Moodie, Etheridge & Humphreys, 1996). The three-beam solution also allows inversion based on the fine structure in convergent-beam electron diffraction (CBED) high-order Laue-zone (HOLZ) lines (Allen & Rossouw, 1993). Certain seven-beam cases in noncentrosymmetric crystals have been reduced to two-beam form (Moodie & Whitfield, 1994).

A direct inversion method would offer great advantages in speed over trial-and-error forward computation methods, in addition to providing a general method for the determination of unknown crystal structures. Because multiple scattering renders the diffracted Bragg intensities sensitive to structure-factor phases, such a method also solves the phase problem of crystallography. Since the method is based on electron microdiffraction patterns, submicrometer crystal volumes can be analyzed. In an earlier paper (Spence, 1978), the use of overlapping coherent orders was analyzed for this purpose and the errors introduced by multiple scattering estimated. The purpose of this paper is to provide a direct nonperturbative solution to the N-beam inversion problem, assuming only that large matrices can be diagonalized by computation. The practical implementation of the scheme is briefly outlined.

2. Forward-scattering theory

The multiple diffraction of a collimated kilovolt electron beam traversing a thin slab of crystal was first described by Blackman (1939), who applied the Bethe multiple-scattering theory (Bethe, 1929) to the transmission or Laue geometry. Many modern treatments have since been presented (Hirsch, Howie, Nicholson, Pashley & Whelan, 1977; Humphreys, 1979; Spence & Zuo, 1992). A useful form of this Bloch-wave theory is the scattering-matrix approach of Niehrs (1959) and Sturkey (1962), which we adopt here with the formalism of Speer, Spence & Ihrig (1990). We consider only a two-dimensional projection of the crystal potential in the beam direction [zero-order Laue-zone (ZOLZ) reflections]. We exclude inelastic processes and absorption initially. The solution inside the crystal of the relativistically corrected Schroedinger equation may be expanded over reciprocal-lattice vectors $\mathbf{g}$ as a sum of Bloch waves of the form

$$\psi^{(j)}(\mathbf{r}) = \sum_g C_g^{(j)}(\mathbf{k}^{(j)}) \exp[2\pi i(\mathbf{k}^{(j)} + \mathbf{g}) \cdot \mathbf{r}]. \quad (1)$$

Inserting this, together with a Fourier expansion of the periodic crystal potential $V(\mathbf{r})$, into the Schroedinger equation shows that the Bloch-wave expansion coefficients $C_g(\mathbf{k})$ satisfy the dispersion equations

$$[K^2 - (\mathbf{k} + \mathbf{g})^2]C_g(\mathbf{k}) + \sum_{h \neq 0} U_h C_{g-h}(\mathbf{k}) = 0. \quad (2)$$

Here, $K^2 = (2meE/h^2) + U_o$ is the squared mean wavevector of the electron inside the crystal (corrected

for the effect of the average electrostatic potential U_o) and eE is the beam energy. It can be shown (Saldin & Spence, 1994) that, for beam energies sufficiently high to allow the neglect of exchange and virtual inelastic scattering effects (Rez, 1978), the electron beam is diffracted by the electrostatic Coulomb potential alone, which has Fourier coefficients $V_\mathbf{g} = h^2 U_\mathbf{g}/(2me)$. Excitation errors

$$s_\mathbf{g} = (-2\mathbf{K}_t \cdot \mathbf{g} - \mathbf{g}^2)/2K \quad (3)$$

may be defined in the high-energy approximation, where $\mathbf{K}_t$ is the component of the mean wavevector in the plane of the crystal slab, running from the center of the Laue circle to the origin of reciprocal space. If backscattered waves are neglected, the locus of allowed Bloch-wave labeling wavevectors $\mathbf{k}^{(j)}$ may be defined by $\gamma^{(j)} = k_z^{(j)} - K_z$, with the x and y components of $\mathbf{k}^{(j)}$ fixed by boundary conditions. The solutions of equation (2) may then be written in terms of $\gamma^{(j)}$ and $s_\mathbf{g}$ as the family of eigenvalue equations

$$(s_g - \gamma^{(j)})C_g^{(j)} + \sum_{h \neq 0} F_h C_{g-h}^{(j)} = 0 \quad (4)$$

or

$$\mathbf{A}C^{(j)} = \gamma^{(j)}C^{(j)}, \quad (5)$$

where the structure matrix $\mathbf{A} = \mathbf{A}(\mathbf{K}_t)$ contains structure factors $F_{\mathbf{gh}} = U_{\mathbf{g-h}}/2K$ in off-diagonal positions and diagonal elements $s_\mathbf{g}$. (Appendix A provides an example.) Here, $s_\mathbf{g}$, $C_\mathbf{g}^{(j)}$ and $\gamma^{(j)}$ are all functions of the beam direction $\mathbf{K}_t$. For centrosymmetric crystals, $F_{\mathbf{gh}} = F_{\mathbf{hg}}$ may be chosen real if a suitable origin is taken, $\mathbf{A}$ is symmetric and, for the systematic orientation, entries along any sub- or superdiagonal are equal. $C^{(j)}$ is a column eigenvector whose elements are the real quantities $C_\mathbf{g}^{(j)}$. For noncentrosymmetric (acentric) crystals, $F_{\mathbf{gh}} = F_{\mathbf{hg}}^*$ are complex, $\gamma^{(j)}$ are real, $\mathbf{A}$ is Hermitian and $C_\mathbf{g}^{(j)}$ are complex.

Imposition of boundary conditions appropriate to a parallel-sided slab allows the column vector $\varphi_\mathbf{g}$ containing the Bragg beam amplitudes diffracted by a thin crystal of thickness t to be written as a unitary transformation

$$\varphi_\mathbf{g} = \mathbf{S}\varphi_\mathbf{o} \quad (6)$$

in the absence of absorption, where (Hirsch $et\ al.$, 1977)

$$\mathbf{S} = \mathbf{C}[\mathbf{L}]\mathbf{C}^{-1} = \exp(2\pi i \mathbf{A}t) \quad (7)$$

with $\mathbf{C}$ an orthogonal matrix of eigenvectors $C^{(j)}$ and $\mathbf{L}$ a diagonal matrix whose jth element is $\lambda^{(j)} = \exp(2\pi i \gamma^{(j)}t)$. The column vector $\varphi_\mathbf{o}$, describing the incident wave, contains zeros everywhere except for a central entry of unity in the symmetric orientation.

In the absence of absorption, the scattering matrix $\mathbf{S} = \mathbf{S}(\mathbf{K}_t, \mathbf{t})$ is complex, symmetric, orthogonal and unitary

for centrosymmetric crystals, with complex eigenvalues $\lambda^{(j)}$ of unit modulus. S is also centrosymmetric in the systematics orientation. Since C is orthogonal, $C^{-1} = C^T$. For noncentrosymmetric crystals without absorption, S is complex, orthogonal, unitary and symmetric (but A is Hermitian). C is complex but not symmetric. The eigenvalues γ are real in both these cases. For centrosymmetric crystals with absorption, S is complex, symmetric, not unitary or orthogonal and γ are complex. For noncentrosymmetric crystals with absorption, S is neither symmetric nor unitary and γ are complex.

The inversion of dynamical amplitudes from a single data set is seen to be impossible, since the addition of n/t to the eigenvalues $\gamma^{(j)}$ of A (with n a different integer for each $\gamma^{(j)}$) leaves S unchanged but alters the structure factors of the crystal. Inversion from a single data set is therefore not unique (as may be understood from a study of the complex logarithm function), so that several different crystals could, in principle, give rise to identical dynamical diffraction patterns at one thickness (but not at every thickness).

3. Inversion – systematics

The principle of the method is explained most clearly for the systematics orientation where a single line of reflections is simultaneously excited. Then a simple relationship exists between the Miller indices of a beam and the indices of the scattering matrix. The method is extended to two-dimensional patterns and noncentrosymmetric crystals with limited absorption effects in later sections. Let G be a diagonal matrix whose jth element is $\gamma^{(j)}$. From equation (5), the wanted matrix of structure factors

$$A = C[G]C^{-1} \qquad (8)$$

can be found if the eigenvectors C of S and the corresponding eigenvalues $\gamma^{(j)}$ in G can be found. We discuss each of these problems in turn, assuming that the crystal thickness t and the excitation errors are known. Now the eigenvectors C of A are also those of S, so that, if all of complex S can be found, C [and $\lambda^{(j)}$] can be found by diagonalizing S. However, one electron diffraction pattern provides only the modulus squared of the entries in a single column (and row) of S. In the symmetric systematics orientation ($K_t = 0$), for example, only the central element of the column vector φ_0 [in equation (6)] describing the incident beam is nonzero and the complex dynamical Bragg scattering amplitudes ϕ_g are therefore equal to the central row and column of $S(K_t = 0)$, since S is symmetric. Our general approach is to use certain periodicity relations among the eigenvectors and eigenvalues to show that the remaining required columns in S are given by the Bragg amplitudes diffracted by the crystal in certain new orientations. This leaves two problems remaining: firstly, the problem of

determining the complex entries ϕ_g in S (rather than the $|\phi_g|^2$ obtainable from experimental intensities) and, finally, the problem of finding the $\gamma^{(j)}$ values for G in equation (8) from the eigenvalues $\lambda^{(j)}$ of S. An experimental coherent convergent-beam diffraction arrangement with overlapping orders is shown to result in interference between the elements of adjacent columns of $S(K_t = 0)$, so that, by a succession of tilting experiments, all of complex $S(K_t = 0)$ may be found. This allows the eigenvectors of S (which are also those of A) to be obtained. Finally, we use the thickness- (or electron-wavelength-) dependence of the eigenvalues $\lambda^{(j)}(t)$ to obtain unique estimates of the eigenvalues $\gamma^{(j)}$ of A. Equation (8) then gives the wanted structure matrix, from which the crystal charge density may be obtained by Fourier synthesis.

First consider finding the missing elements of S. In the following, we show that these may be found by tilting the crystal. In the symmetric orientation for systematic reflections, S is symmetric, complex and orthogonal. For centrosymmetric crystals, it is also centrosymmetric, with the typical form

$$\begin{bmatrix} a & b & c \\ b & d & b \\ c & b & a \end{bmatrix}. \qquad (9)$$

For noncentrosymmetric crystals in the systematic orientation (without absorption), S is symmetric rather than centrosymmetric and we discuss that case below. The properties of centrosymmetric matrices are discussed elsewhere (Cantoni & Butler, 1976); they possess equal numbers of odd and even eigenvectors. An $N \times N$ centrosymmetric matrix (corresponding to N beams) contains $(N + 1)^2/4$ distinct entries, thus the entire matrix can be obtained from a knowledge of one quadrant. According to Bloch's theorem, the wavefunction in (1) is periodic in reciprocal space, since all solutions of the wave equation for the general wavefield inside the crystal may be defined within the first Brillouin zone (Metherell & Fisher, 1969). In consequence,

$$C_g^{(j)}(\mathbf{k}^{(j)}) = C_{g+h}^{(j)}(\mathbf{k}^{(j)} - \mathbf{h}). \qquad (10)$$

Since the x components of $\mathbf{k}$ and $\mathbf{K}_t$ are equal, this equation relates eigenvector elements between two orientations that differ by the addition of a reciprocal-lattice vector to $\mathbf{K}_t$, the vector defining the center of the Laue circle. For $\mathbf{K}_t = \mathbf{k}_x = 0$ (symmetric orientation), the right-hand side of (10) refers to the second-order Bragg condition along the systematics line where $\mathbf{h}$ is the first-order reflection and $\mathbf{K}_t = -\mathbf{h}$. A second periodicity condition exists for similar reasons amongst eigenvalues. Because of the periodicity of the dynamical dispersion surfaces (Høier, 1972), we have

$$\gamma^{(j)}(\mathbf{k} - \mathbf{h}) = \gamma^{(j)}(\mathbf{k}) + s_\mathbf{h}. \qquad (11)$$

With these results, it is possible to compute the diffracted wavefield for any orientation from a knowledge of $C_g^{(j)}(\mathbf{K}_t)$ and $\gamma^{(j)}(\mathbf{K}_t)$ for values of $\mathbf{K}_t$ given within the first Brillouin zone only. It follows that the nonobservable elements in $\mathbf{S}(\mathbf{K}_t = 0)$ are equal to observable elements in $\mathbf{S}(\mathbf{K}_t = \mathbf{h})$. For example, consider the three-beam systematics case with beams $-\mathbf{h}$, 0, $\mathbf{h}$. If primes are used to denote the tilted orientation $\mathbf{K}_t = -\mathbf{h}$ at the second-order Bragg condition, the central element of the scattering matrix S_{22} becomes, from (7),

$$S'_{22} = (C_0''^{(1)})^2 \exp\{2\pi i[\gamma'^{(1)}(0) + s_h]t\}$$
$$+ (C_0''^{(2)})^2 \exp\{2\pi i[\gamma'^{(2)}(0) + s_h]t\}$$
$$+ (C_0''^{(3)})^2 \exp\{2\pi i[\gamma'^{(3)}(0) + s_h]t\}, \quad (12)$$

while the element in the third row and second column is

$$S'_{32} = C_h''^{(1)}C_0''^{(1)} \exp\{2\pi i[\gamma'^{(1)}(0) + s_h]t\}$$
$$+ C_h''^{(2)}C_0''^{(2)} \exp\{2\pi i[\gamma'^{(2)}(0) + s_h]t\}$$
$$+ C_h''^{(3)}C_0''^{(3)} \exp\{2\pi i[\gamma'^{(3)}(0) + s_h]t\}. \quad (13)$$

The phase factor $\exp(2\pi i s_h t)$ is common to all terms in the matrix ($\mathbf{h} = \mathbf{K}_t$ is not a variable) and so does not affect phase differences between beams. Applying (10) in the form $C_{\mathbf{g}-\mathbf{h}}^{(j)}(\mathbf{K}_t = 0) = C_{\mathbf{g}}''^{(j)}(\mathbf{K}_t = -\mathbf{h})$ to (12) gives

$$S'_{22} = [(C_{-h}^{(1)})^2 \exp(2\pi i\gamma^{(1)}t) + (C_{-h}^{(2)})^2 \exp(2\pi i\gamma^{(2)}t)$$
$$+ (C_{-h}^{(3)})^2 \exp(2\pi i\gamma^{(3)}t)] \exp(2\pi i s_h t),$$

where $\gamma^{(j)} = \gamma^{(j)}(0)$. Apart from the last phase factor, this is equal to the term S_{11} in the matrix describing the symmetric orientation $\mathbf{K}_t = 0$. Similarly, (13) becomes

$$S'_{32} = [C_0^{(1)}C_{-h}^{(1)} \exp(2\pi i\gamma^{(1)}t) + C_0^{(2)}C_{-h}^{(2)} \exp(2\pi i\gamma^{(2)}t)$$
$$+ C_0^{(3)}C_{-h}^{(3)} \exp(2\pi i\gamma^{(3)}t)] \exp(2\pi i s_h t), \quad (14)$$

which is equal to element S_{21} for the symmetric orientation. In general, if the beams of the systematics line are indexed as $n\mathbf{g}$, then $S_{pq}(\mathbf{K}_t = n\mathbf{g}) = S_{p-n,\ q-n}(\mathbf{K}_t = 0)$. Entries in the scattering matrix $\mathbf{S}'$ for a tilted orientation $\mathbf{K}_t = n\mathbf{h}$ correspond to those in the matrix for the symmetric orientation if shifted in $\mathbf{S}'$ by n places to the left (for example) along the direction of the diagonal. This moves an entry in $\mathbf{S}'(\mathbf{K}_t = n\mathbf{h})$ to the position of the same entry in $\mathbf{S}(\mathbf{K}_t = 0)$. Positive and negative tilts (values of $\mathbf{K}_t$) move entries in opposite senses parallel to the diagonal and are equivalent for centrosymmetric crystals. Conversely, we may consider that each tilt by $\mathbf{K}_t = n\mathbf{h}$ moves that column vector $\mathbf{X}$ in $\mathbf{S}(\mathbf{K}_t = 0)$ which lies n columns to the left of the central column into the central position for observation. $\mathbf{X}$ is also moved n positions downward. This is indicated schematically in Fig. 1, which shows the form of the centrosymmetric matrix for the seven-beam case in the symmetric orientation ($\mathbf{K}_t = 0$). The upper quadrant

(shaded) indicates the $(N+1)^2/4 = 16$ distinct complex entries. The columns on the left of the central column are labeled below by the orientation that will bring them into the central observable position [e.g. $\mathbf{g}_1 = (111)$, $\mathbf{g}_2 =$
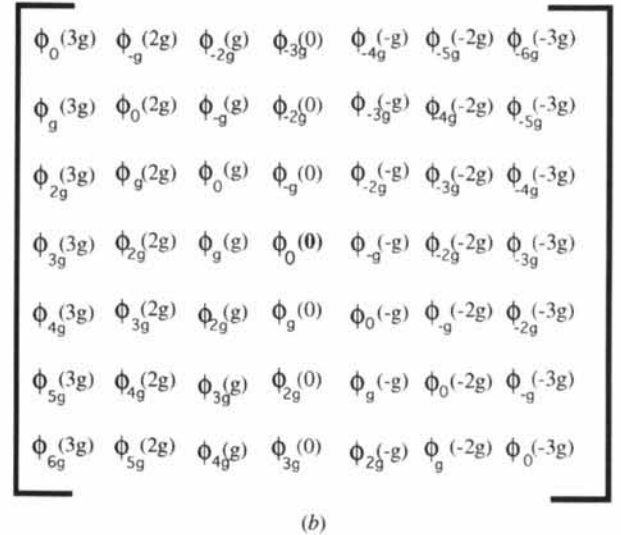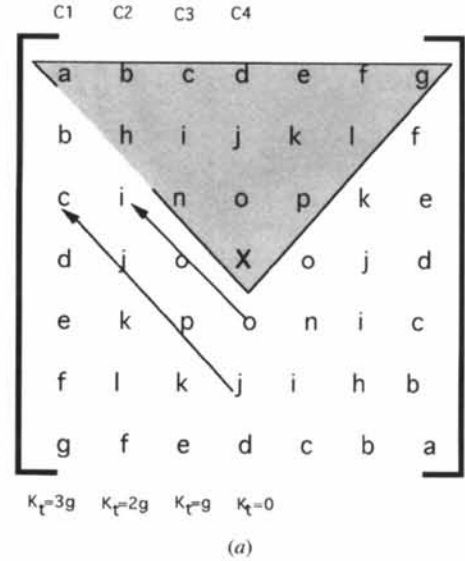

(a)

(b)

Fig. 1. (a) The centrosymmetric scattering matrix for a centrosymmetric crystal in the symmetric systematics orientation. Only elements in the upper shaded triangle are distinct; only the central column is observable. Element o in the observable central column of the matrix for tilted condition $\mathbf{K}_t = 2\mathbf{g}$ is equal to element i in the matrix for the symmetric orientation. Similarly for j and c. Hence, experiments which interfere o and j give phase differences between elements in rows $C1$ and $C2$ of the matrix for the symmetrical orientation. (b) The same matrix $\mathbf{S}$ for the symmetric systematics orientation but with entries labeled by the amplitudes of diffracted beams occurring in tilted conditions. The quantity in parentheses is the value of $\mathbf{K}_t$, which defines the beam direction. These amplitudes are equal to those in $\mathbf{S}$ apart from certain phase factors. Not all elements are distinct, since the matrix is symmetric and centrosymmetric. Here $\mathbf{g}$ is the first-order Bragg reflection.

(222), $\mathbf{g}_3 = (333)$ *etc.*]. These results arise because the effect of tilt is to move all elements down one position in $\mathbf{C}$ in (7) and hence across one position in the transpose $\mathbf{C}^T = \mathbf{C}^{-1}$, resulting in a diagonal movement in $\mathbf{S}$. The effect of tilt on the eigenvalues can also be understood by noting that the tilted set of excitation errors can be obtained from the symmetric orientation by moving them all along one place on the diagonal of $\mathbf{A}$ and adding an unimportant constant. In all experiments (for all tilts), because of our arrangement of the diagonal of $\mathbf{A}$, only the central column of $\mathbf{S}$ or $\mathbf{S}'$ is observable.

Now consider the experimental arrangement shown in Fig. 2. This shows the diffraction conditions for coherent convergent-beam diffraction, with interference between overlapping orders, which can be set up on modern field-emission STEM instruments (see Spence, 1978; Spence & Cowley, 1978; Cowley, 1986; Zuo & Spence, 1993; McCallum & Rodenberg, 1992). High-contrast interference fringes are also seen between overlapping orders on modern FEG TEM/STEM instruments, as demonstrated recently by Vincent, Vine, Midgley, Spellward & Steeds (1992), Tanaka, Terauchi & Tsuda (1994) and others. Using the preceeding result, it will now be shown that the intensity at points such as D can be described by interference between neighboring matrix elements in the
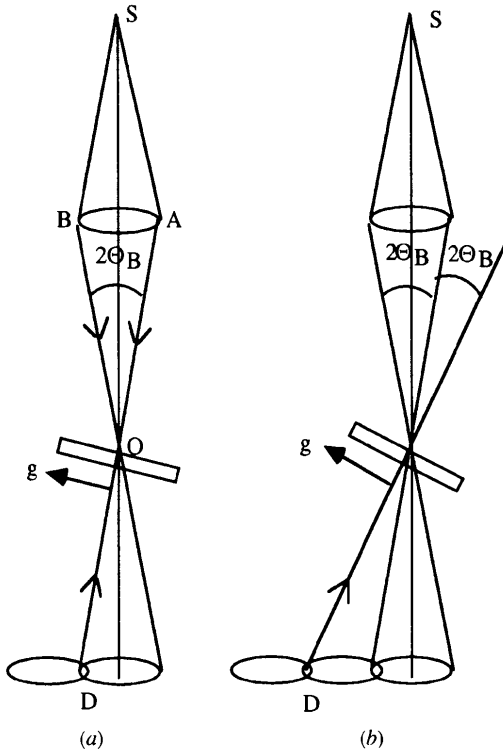

Fig. 2. Diffraction conditions in coherent STEM which allow the phases of matrix elements in the scattering matrix to be determined. (a) produces interference between columns $C4$ and $C3$ in Fig. 1, while (b) gives interference between $C2$ and $C3$. The direction of the systematics line is indicated by $\mathbf{g}$ in each case.

same row of $\mathbf{S}(\mathbf{K}_t = 0)$. We assume that the illumination aperture is coherently filled, so that interference occurs between optical paths AOD and BOD. Because only scattering through multiples of twice the Bragg angle is allowed, the amplitude at D is the sum of the direct beam AOD, $\phi_0(\mathbf{K}_t = 0)$, in the symmetric orientation, and the first-order diffracted beam BOD, $\phi_g(\mathbf{K}_t = -\mathbf{g})$ at the second-order Bragg condition. If the beams of the systematic line are labeled with an integer index m and $g = 1/d$, where d is the first-order lattice spacing, then the complex amplitude recorded at D in Fig. 2(a) is (with $m = n = 0$)

$$
\begin{aligned}
\Psi_D(x) &= \phi_n(\mathbf{K}_t = -m\mathbf{g})\exp(2\pi i n g x) \\
&\quad + \phi_{n+1}[\mathbf{K}_t = -(m+1)\mathbf{g}]\exp[2\pi i(n+1)gx] \\
&= \sum_i C_0'^{(i)}C_{ng}'^{(i)}(\mathbf{K}_t = -m\mathbf{g})\exp[2\pi i(\gamma'^{(i)}t + ngx)] \\
&\quad + \sum_i C_0'^{(i)}C_{(n+1)g}'^{(i)}[\mathbf{K}_t = -(m+1)\mathbf{g}] \\
&\quad \times \exp\{2\pi i[\gamma'^{(i)}t + (n+1)gx]\}. \qquad (15)
\end{aligned}
$$

In Fig. 2(b), a crystal tilt $\mathbf{K}_t = -\mathbf{g}$ has been applied. The preceding equation describes the case of a general tilt $\mathbf{K}_t = -m\mathbf{g}$ for reflection $n\mathbf{g}$. Then, n is the row index of the matrix element in the central column of the scattering matrix for the inclined orientation. Applying (10) [in the form given after equation (13)] and (11) gives an expression in terms of the scattering matrix for the symmetric orientation:

$$
\begin{aligned}
\Psi_D(x) &= \sum_i C_{-mg}^{(i)}C_{(n-m)g}^{(i)}(0) \\
&\quad \times \exp(2\pi i\{[\gamma^{(i)}(o) + s_{mg}]t + ngx\}) \\
&\quad + \sum_i C_{-(m+1)g}^{(i)}C_{(n-m)g}^{(i)}(0) \\
&\quad \times \exp(2\pi i\{[\gamma^{(i)}(o) + s_{(m+1)g}]t + (n+1)gx\}).
\end{aligned}
$$

$$(16)$$

Here the subscript of the first C in each pair is the column index in the scattering matrix for the symmetric orientation and the subscript of the second C is the row index, in terms of the original beam index and tilt (see Fig. 1a). We define

$$
C_{H,G}(0)\exp(\theta_{H,G}) = \sum_i C_{Hg}^{(i)}(0)C_{Gg}^{(i)}(0)\exp[2\pi i\gamma^{(i)}(o)],
$$

$$(17)$$

where $H = -m$ and $G = n-m$ are the row and column indices in the matrix for the symmetric orientation. Then,

$$
\begin{aligned}
\Psi_D(x) &= C_{H,G}(0)\exp[2\pi i(s_{-Hg}t + ngx) + i\theta_{H,G}] \\
&\quad + C_{(H-1),G}(0)\exp\{2\pi i[s_{(-H+1)g}t + (n+1)gx] \\
&\quad + i\theta_{(H-1),G}\}. \qquad (18)
\end{aligned}
$$

The intensity is

$$I_D(x) = |C_{H,G}|^2 + |C_{H-1,G}|^2 + 2C_{H,G}C_{H-1,G}$$
$$\times \cos[2\pi(\Delta St + gx) + \theta_{H,G} - \theta_{(H-1),G}], \qquad (19)$$

where $\Delta S = S_{-H} - S_{-H+1}$. We may thus interpret the result of the experiments shown in Fig. 2 as providing interference between columns H and $H - 1$ of the scattering matrix for the symmetric orientation $S(\mathbf{K}_t = 0)$. The set of all overlaps in Fig. 2(a), for example, is described by interference between the elements of the central column $C4$ of $S(\mathbf{K}_t = 0)$ and the neighboring column $C3$ – each overlap defines a different row. For example, at D in Fig. 2(a), interference occurs between elements X and o (in row 4) of Fig. 1(a), while the next overlap along the systematic line [not shown in Fig. 2(a)] involves interference between elements o (in $C4$) and element p in $C3$. In Fig. 2(b), the crystal has been tilted to a new Bragg condition, so the set of all overlaps is now described by interference between $C3$ and $C2$, and so on.

To further clarify this, in Fig. 1(b) the scattering matrix for the symmetric orientation $S(\mathbf{K}_t = 0)$ has been redrawn with the entries replaced by the amplitude of diffracted beams scattered under various even-order Bragg conditions. Quantities in parentheses indicate values of $\mathbf{K}_t$. We see that the complex amplitudes at the midpoints of overlapping orders in Fig. 2(a) consist of the interference between elements of columns 3 and 4 of this matrix; for example, (15) (with $m = n = 0$) describes interference between elements of the central row in columns three and four. Similarly, the experiment shown in Fig. 2(b) involves interference between the second and third columns, and so on. Since only the central column of S is observable (for any tilt), arrows have been drawn in Fig. 1(a) that show how a pair of adjacent reflections in the observable central column appear in adjacent columns (end of arrow) in the scattering matrix $S(\mathbf{K}_t = 0)$ for the axial orientation. Each reflection (o and j in the central column) is referred to a different orientation, and therefore both contribute to the intensity at a point such as D in Fig. 2(a). Thus, the phase differences between elements of the same row but different columns may all be measured in pair-wise fashion using tilting experiments – a kind of dynamical 'stepping out' (Spence, 1978; McCallum & Rodenberg, 1992). If S is symmetric, so that the central row equals the central column, this is sufficient to phase the entire scattering matrix. Then the eigenvalues and eigenvectors of $S(\mathbf{K}_t = 0)$, needed for (8), can be found.

A complication arises, however, because the intensity in (19) depends on the relative position x of the coherent probe within the first-order lattice spacing $d = 1/g$. All interferences between each *pair* of adjacent columns in the scattering matrix are obtained for the same probe position at a given tilt. The question then arises as to how the analysis is affected by the inevitable changes in probe

position relative to the crystal (on an atomic scale), which will accompany changes in crystal orientation as one attempts to phase successive pairs of columns in S. Before considering this, we note that the effect of lens aberrations cancels at the midpoint of the overlap (Zuo & Spence, 1993). The arrangement is equivalent, by reciprocity, to 'aberration-free' two-beam lattice imaging with inclined illumination, for which a stationary-phase focus condition may be selected to allow use of the largest possible detector (Spence & Cowley, 1978). The fringes formed within the overlap region can also be interpreted as a point-projection shadow image (or in-line electron hologram) of the crystal lattice (Zuo & Spence, 1993). The amplitudes $C_{H,G}$ and $C_{H-1,G}$ may be obtained (with an ambiguity of sign) from intensity measurements with a smaller illumination aperture which prevents overlap of orders. The intensity $I_D(x)$ at the midpoint of all the overlapping orders may then be measured simultaneously as a function of x (for a particular value of the column index H) as the STEM probe is scanned in the direction of the systematics line. The relative phase delays of these sinusoidal curves give the difference between the differences $\Delta\Theta_{HG} = \Theta_{H,G} - \Theta_{(H-1),G}$. Equation (19) may also be inverted for a particular value of x to give the quantities $(2\pi gx + \Delta\Theta_{HG})$, since ΔS is known and the amplitudes C can be measured.

Because of the symmetry of the matrix, fixing one phase (corresponding to a choice of origin) then determines the phase of every entry in $S(\mathbf{K}_t = 0)$, according to (19). For example, assume initially that *all* phase differences for every pair of columns could be measured for the same value of probe position x. Then a knowledge of all differences along the central row, together with the definition of, say, $(\vartheta_{0,0} + 2\pi gx)$, fixes all phases along this row. This then fixes all values along the central column, since S is symmetric. Since the differences between elements in the same row and adjacent columns are also known, the entire complex scattering matrix can be found.

In fact, however, movement of the crystal with respect to the probe during the tilting operation (on the scale of the unit cell) is inevitable and must be allowed for by introducing separate values of the probe positional phases, for every tilt, as free parameters. Then, in more detail, the measured arguments of the cosine functions in (19) define a system of linear equations. Assume that these arguments are measured for a series of tilts, each with a different probe position $x_i = dp_i/2\pi$ (and probe 'phase' p_i). Then, in the seven-beam case, the interference between columns four and five of S in Fig. 1(a) gives measurements

$$b_1 = p_0 + \Theta_d - \Theta_e$$
$$b_2 = p_0 + \Theta_j - \Theta_k$$
$$b_3 = p_0 + \Theta_o - \Theta_p$$
$$b_4 = p_0 + \Theta_X - \Theta_o \quad \text{etc.}$$

and

$$b_9 = p_1 + \Theta_e - \Theta_f$$

$$b_{10} = p_1 + \Theta_k - \Theta_l$$

$$b_{11} = p_1 + \Theta_p - \Theta_k$$

$$b_{12} = p_1 + \Theta_o - \Theta_j \quad etc.$$

for columns five and six, and similarly for columns six and seven, with probe phase p_2. Additional equations could be generated (but are not needed) by the difference between the differences, obtained from a comparison of the sinusiodal $I_D(x)$ curves for different overlaps. We may then establish an origin by assuming $p_0 = 0$. Because of the symmetry of S, which ensures that the same elements occur in different columns, this system of linear equations

$$\mathbf{Dx} = \mathbf{b} \tag{20}$$

(with x and b column vectors) may be solved by standard methods. Here, x contains the phases Θ and relative probe positions p_i, while b contains the measured cosine arguments. The coefficient matrix **D** is sparse, contains only values 0, ± 1, is not singular and has a condition number of about 10 in typical cases. In general, for a centrosymmetric crystal, there are $(N + 1)^2/4$ distinct entries in S, together with $(N + 1)/2 - 1$ probe phases, giving fewer unknowns than the number $N(N + 1)/2$ of equations (difference–difference equations not included). In this way, using one tilt setting of the crystal for every column in S, all of the complex entries in the scattering matrix $S(\mathbf{K}_t = 0)$ may be found and hence its eigenvalues $\lambda^{(i)}$ and eigenvectors C_j. In summary, because the crystallographic part of each phase occurs at least twice, in different positions in the symmetric scattering matrix, there is enough information to solve for the probe positional phases, which differ for every pair of columns in S.

With modern computer-controlled goniometers and probe scanning, the collection of data from a set of such diffraction conditions might be automated. The crystal must be tilted successively to direct its zone axis to the midpoint of every overlapping pair of diffraction discs in the pattern and, for each of these tilts, the entire set of midpoint intensities must be recorded, perhaps as a function of electron probe position. Note that the electron optical conditions remain unchanged as the crystal is tilted, so that the optic axis always bisects the incident beams, causing aberrations to cancel. It is a remarkable feature of this arrangement that, because only the interference between neighboring orders is used, the phase of very high orders can be obtained, despite the use of a probe whose width is much larger than the d spacing of these high orders. Thus, the coherence angle $2\Theta_B$ needed may be much smaller (equal to only twice the first-order Bragg angle) than the Bragg angle for the highest-order reflections phased (e.g. Fig. 2b), with a

consequent relaxation in demands on electron source size and electronic stability. The amplitude and phase of structure factors may thus be determined for orders of diffraction that are well beyond the image resolution limit of the electron microscope used (Nellist & Rodenberg, 1994; Nellist, McCallum & Rodenberg, 1995). A resolution limitation may occur, however, owing to the decreasing intensity of high-order reflections in the region of overlap – these reflections at this point are far from the Bragg condition (see Fig. 2). The use of a higher accelerating voltage to 'flatten' the Ewald sphere will reduce this effect.

The inversion, based on equation (8), is finally completed by finding the real quantities $\gamma^{(j)}$ from the complex thickness-dependent eigenvalues of S(t),

$$\lambda^{(j)}(t) = \exp(2\pi i \gamma^{(j)}t) = \cos(2\pi\gamma^{(j)}t) + i \sin(2\pi\gamma^{(j)}t). \tag{21}$$

This may be performed, and a unique inversion ensured, by plotting, say, $\mathrm{Im}\{\lambda^{(j)}(t)\} = \sin(2\pi\gamma^{(j)}t)$ against thickness and noting the period $(\gamma^{(j)})^{-1}$ of the resulting function. [These periods are not extinction distances $(\gamma^{(i)} - \gamma^{(j)})^{-1}$, however a reflection at the Bragg condition shows an approximate period $(2\gamma^{(j)})^{-1}$.] Ideally, measurements of S(t) and $\lambda^{(j)}(t)$ at just two thicknesses are sufficient to fix the amplitude and maximum period of all $\lambda^{(j)}(t)$. However, in the presence of noise and absorption (discussed below), several thicknesses will be needed. We note that an arbitrary experimental phase shift applied to the incident beam ϕ_o [equation (6)] in data collected at a second thickness does not affect the eigenvalues of S, so that the absolute phase difference between measurements made at different thicknesses is not required.

An important point of detail arises also in the ordering of the eigenvalues. Diagonalization of a series of
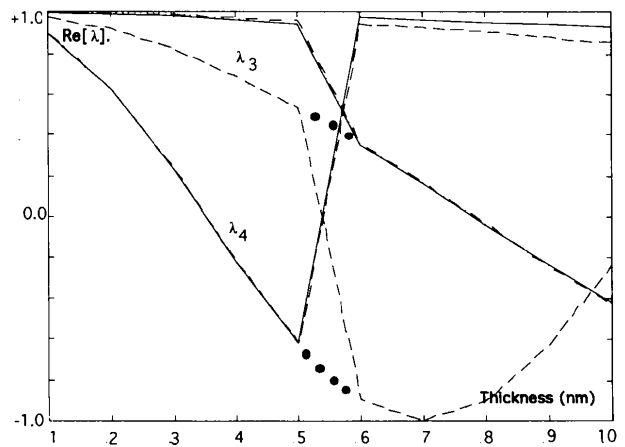

Fig. 3. Real part of eigenvalue of scattering matrix S plotted against thickness for aluminium (111) systematics at 1 MeV. These are cosine curves. The ordering of the eigenvalue labels changes at 5.5 nm thickness; black dots indicate the required uninterrupted ordering.

complex matrices $S(t)$ will produce eigenvalues whose ordering may abruptly change at certain thicknesses. However, the continuity of the function $\lambda^{(j)}(t)$ can be used to determine the correct ordering as a continuous function of thickness. Fig. 3 shows a seven-beam simulation for the case of the (111) systematic reflections in aluminium at 1 MeV. The real part of $\lambda^{(j)}(t) = \cos[2\pi\gamma^{(j)}t]$ is plotted as a function of thickness for several eigenvalues. At a thickness of 55 Å, the ordering of the eigenvalues returned by the 'Eispack' routine (Smith, 1976) alters; however, it is clear from the continuity requirement (shown by black dots) that, for example, above this thickness $\lambda^{(3)}$ should be re-labeled $\lambda^{(4)}$. Other crossings are evident.

A simpler method may be to use patterns collected at two accelerating voltages, which, nonrelativistically, is equivalent to a change in thickness Δt. Then, the $\gamma^{(j)}$ may be found uniquely by differentiation, using, from equation (21),

$$\frac{\Delta\lambda^{(j)}}{\Delta t \lambda^{(j)}} \simeq \frac{\partial\lambda^{(j)}}{\partial t}\frac{1}{\lambda^{(j)}} = 2\pi i \gamma^{(j)}.$$

Having obtained the complete complex scattering matrix (and hence its eigenvectors) from a series of tilting experiments, and the corresponding set of eigenvalues from the thickness or wavelength dependence of $S(t)$, the structure matrix A containing the wanted structure factors may be obtained using (8).

4. Two-dimensional patterns

The preceding approach may be extended to the analysis of two-dimensional cross-grating or ZOLZ diffraction patterns in a straightforward way, however the relationship between the Miller indices of the diffraction spots and matrix indices must be determined and the shape of the illumination aperture considered. The central column of $S(K_t = 0)$ now contains all the reflections in the two-dimensional pattern. Other columns describe two-dimen-

sional patterns from crystal orientations differing by $K_t = g$, where g is any reciprocal-lattice vector. Fig. 4 shows the general two-dimensional lattice A_o (P1). The lattice formed from this by the midpoints of the overlap of all neighboring diffraction discs is not identical to A_o, rather it is centered and contains additional points B. No Bragg scattering can occur between these two sublattices. Only one sublattice of points is required to phase the scattering matrix, since K_t values within the illumination aperture terminating at A and B do not differ by a reciprocal-lattice vector. (Points B could be eliminated by using an elliptical illumination aperture.)

Fig. 5 illustrates the application of the two-dimensional form of equation (19) to a ZOLZ pattern for interference between reflections g and, in a second orientation, $(g + h)$. The intensity recorded at D is

$$I_D(r, \Delta\theta_{g \cdot g + h}) = |\phi_g(K_t = 0)|^2 + |\phi_{g+h}(K_t = -h)|^2$$
$$+ 2|\phi_g||\phi_{g+h}|\cos[2\pi(\Delta St + h \cdot r)$$
$$+ \Delta\theta_{g \cdot g + h}]. \tag{22}$$

In order to fill out all of $S(K_t = 0)$ and obtain interference between every pair of columns in $S(K_t = 0)$, it will be found necessary to tilt the crystal by every two-dimensional lattice vector G using a coherently filled illumination aperture that just spans each of the reciprocal-lattice basis vectors. More specifically, K_t must take successively each of the unchanging indices in every column of S and the entire two-dimensional
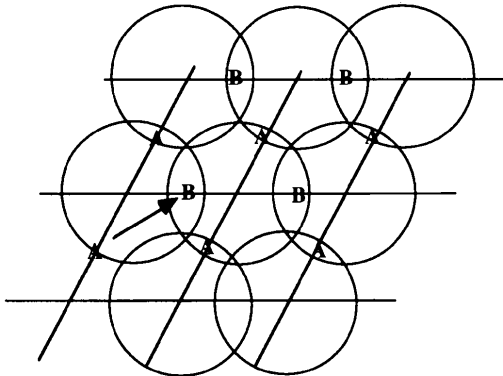

Fig. 4. General two-dimensional lattice with diffraction discs on each site. Bragg diffraction couples all points A and all those labeled B but does not occur between them (arrow).
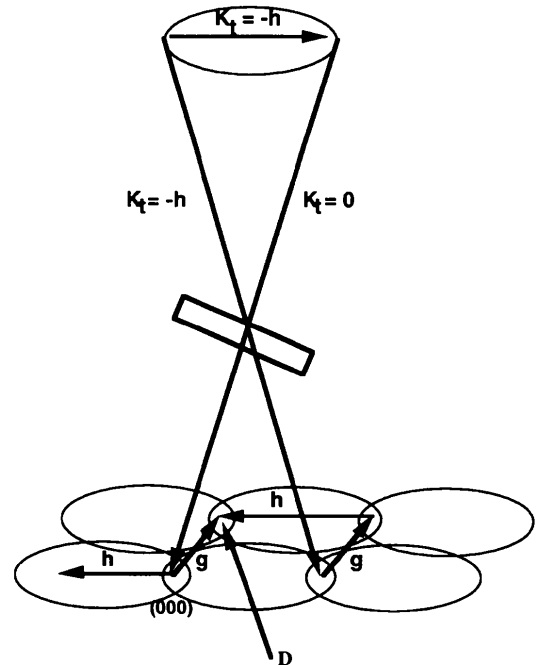

Fig. 5. Schematic indication of dynamical interference between overlapping coherent diffraction orders. The intensity at D is measured as a function of probe position.

pattern recorded in each case. The pattern of overlapping midpoints can be thought of as two point diffraction patterns superimposed after displacement by a lattice vector. Each is described by a different value of $\mathbf{K}_t$, measured from the origin of reciprocal space to the center of the Laue circle, and proportional to the angle between the crystal zone axis and the beam in real space. In general, the complex amplitude at points such as D is given by the sum of elements from the central column of two different scattering matrices $S(\mathbf{K}_t = \mathbf{G})$ and $S(\mathbf{K}_t = \mathbf{G} - \mathbf{h})$, such as o and j in Fig. 1(a). Thus, their interference can be interpreted as occurring between c and i in different columns of $S(\mathbf{K}_t = 0)$. Appendix A contains an indexed example for a face-centered cubic lattice.

The general procedure for inversion using two-dimensional patterns is as follows:

(i) Using standard CBED methods, the space group of the crystal must be found and the ZOLZ pattern corresponding to the projection of the structure required must be indexed (for details, see Spence & Zuo, 1992). The cell dimensions and Bravais lattice can be found accurately by the method of Zuo (1994), which uses the three-dimensional HOLZ lines in the central disc. Crystal thickness can be found to a good approximation, independently of the structure factors, using two-beam analysis (Spence & Zuo, 1992).

(ii) The Miller indices so obtained are set out along the central column of $S(\mathbf{K}_t = 0)$, with (000) in the center and conjugate pairs on either side, and increasing scattering angle away from the center (the order is not critical). Terms $C_g^{(i)}C_0^{(i)}$ may then be assigned to every element of the central column of S. It will be seen from the example given in Appendix A that this is sufficient to assign a pair of Miller indices to every entry in S by inspection. [The example is consistent with equation (7).] The sequence of Miller indices along the central column of S is also that of the diagonal of the structure matrix A and of the central column of A. This defines the Miller indices of all the structure factors in A and hence of those that will be retrieved. (Because of coupling reflections important for multiple scattering, more structure factors are recovered than those defined by the central column of S).

(iii) The crystal must be tilted under computer control so that $\mathbf{K}_t$ is set equal, successively, to the lattice vector defined by the unchanging Miller index in every column of $S(\mathbf{K}_t = 0)$. The illumination aperture must correspond to the difference $\mathbf{a}$ between this vector and that of a neighboring column. For each of the N tilts, the N intensities at the midpoint of all the overlapping discs must be recorded simultaneously as the electron probe is scanned in direction $\mathbf{a}$. This provides the N^2 amplitudes and phases required to fill out S for a noncentrosymmetric crystal. The result of scanning will be a family of sinusoidal curves, one for each midpoint, each with a different relative phase delay, giving the difference between the values of $\Delta\Theta_{g, g+h}$ in (22) and the values

of the cosine arguments for some (initially) unknown probe position x. By scanning over many cells, the signal-to-noise ratio can be improved. The intensities of the spots are also required for every tilt – these can be obtained using a slightly smaller illumination aperture. This procedure can be justified by writing each ϕ_g in terms of $C_g C_0$ [in S', as in equation (15)] and applying the periodicity relation (10). The corresponding pair of indices for this term $C_{g'h'}$ in $S(\mathbf{K}_t = 0)$ can then be found as in the systematics case. Appendix A gives an example for a two-dimensional pattern. The arrows in Fig. 1(a) indicate how this works in practice for the crystal tilts shown below each column.

(iv) Equation (20) must be applied to the experimental data to find the matrix element phases and all probe positions except the first, which defines the origin. The phase factor ΔSt in equation (22) is known and has a different value for each column of S.

(v) This entire proceedure must be repeated for several thicknesses or electron beam energies and the resulting scattering matrices diagonalized. Equation (21) then allows the eigenvalues of the structure matrix A to be obtained from those of S. With these eigenvalues and the eigenvectors of S, (8) gives A containing the wanted electron structure factors U_g.

(vi) The resulting U_g values can be converted to X-ray structure factors and a charge-density map synthesized. This will show projected atomic positions and, from the heights of the peaks, will also give the atomic number of the species. By repeating the procedure for different zones, a three-dimensional structural analysis may be completed.

5. Noncentrosymmetric crystals

For noncentrosymmetric crystals without absorption, A is Hermitian, γ real and S symmetric. Then, S contains $(N + 1)N/2$ distinct entries. The vector of unknown phases $\mathbf{x}$ in (20) then contains this number plus $(N - 2)$ unknown probe positions p_i, which is less than the number of equations $(N - 1)N$. The matrix D in equation (20) is not singular and hence the same method can be applied as for centrosymmetric crystals using two-dimensional patterns. Since phase differences between columns on both sides of the central column in S must be found, twice as many crystal tilts are required as for the centrosymmetric case.

6. Absorption

If inelastic scattering processes are introduced, the corresponding 'absorption' of the elastic wavefield may be included in the approximation of a local inelastic potential by perturbation methods in the independent Bloch-wave model for centrosymmetric crystals (Hirsch et al., 1977) or, more exactly, without making the independent Bloch-wave approximation, through the use

of an optical potential (Rez, 1979). This results, for centrosymmetric crystals, in the addition of small imaginary parts to $F_g = U_g/2K$, so that $\mathbf{A}$ is no longer Hermitian but remains symmetric for centrosymmetric crystals. Since $\mathbf{S}$ is also then symmetric, the preceding method, which requires that $\mathbf{S}$ be symmetric, holds for centrosymmetric crystals including the effects of anomalous absorption. The eigenvalues $\gamma^{(i)}$ are complex in this case, so that the imaginary part of (21) becomes an exponentially damped sinusoid, which may be fitted by modeling.

For noncentrosymmetric crystals with anomalous absorption included, $\mathbf{S}$ and $\mathbf{A}$ are general complex matrices (Bird, 1990; Spence & Zuo, 1992) and the method fails. However, many two-dimensional projections of noncentrosymmetric crystals are centrosymmetric and so can be analyzed. In addition, the dominant contribution to absorption is the mean absorption parameter iF'_{gg} (where $|F'_{gg}| \ll |F_{gg}|$), which is added to all diagonal elements of $\mathbf{A}$. This leaves eigenvectors unchanged, adds iF'_{gg} to all eigenvalues of $\mathbf{A}$ and preserves the orthogonality of $\mathbf{S}$, whose normalization is no longer independent of thickness. $\mathbf{S}$ remains complex and symmetric. Thus, all entries in $\mathbf{S}$ can be obtained with the inclusion of a mean absorption effect. The value of the mean absorption coefficient may be extracted from the eigenvalue period analysis.

Several additional constraints may be applied to improve the accuracy of the inversion. For centrosymmetric crystals, the phases retrieved must all be zero or π and forbidden reflections should be recovered correctly. No use has been made of the space-group information available from preliminary CBED analysis, which relates many amplitudes and phases, imposing additional symmetries on $\mathbf{S}$ and so reducing data-collection time from the centrosymmetric case treated above. The plane group of the various Bloch waves excited can also be determined [see Taftø (1988) in Spence (1988), Fig. 5.7, for a worked example and tables]. In particular, also, the orthogonality requirement for $\mathbf{S}$ imposes a powerful (nonlinear) condition that relates phases obtained from different orientations. This may be applied in cases where the mean absorption coefficient alone is used. Finally, using the known trace of $\mathbf{A}$, we have

$$\sum_j \gamma^{(j)} = \sum_g s_g.$$

7. Discussion

The main purpose of this paper has been to show that the inversion of dynamical intensities is possible in principle (and possibly in practice), given their variation with thickness and crystal orientation under two-beam coherent illumination conditions. Since this inversion procedure is exact, the analysis of simulated data amounts to a study of numerical rounding errors and stability. This can be used to study the effects of noisy data and errors in

experimental parameters, such as thickness and Debye–Waller factors. The method does not provide a closed-form solution, since the diagonalization of matrices of order N is required. Although exact, the method is inefficient in that it takes no account of the strength of the various Bloch waves or beams. The practical implementation of this method depends on computer control of electron microscopes. In particular, using integrated software control of imaging energy filters, CCD cameras and digital goniometers, it may be possible to automate collection of the required data on a field-emission STEM instrument. An imaging energy filter would be essential to reduce background by excluding most inelastic scattering.

The most important practical difficulties are likely to include the effects of noisy data and the large range of periods $L^{(j)} = [\gamma^{(j)}]^{-1}$. For light elements at 100 kV, the periods $L^{(j)}$ range from a few nanometers to a few hundred nanometers. At 1 MeV for light elements, the lower limit increases to tens of nanometers with an upper limit of a few hundred nanometers. Higher accelerating voltages are therefore desirable to increase the shortest periods. The accuracy with which fractional atomic coordinates are determined depends on errors in the structure-factor amplitudes and phases, and this will depend on many factors, including the number of thicknesses used, the number of unit cells scanned over, the neglect of anomalous absorption for noncentrosymmetric crystals, and on the precise location of the Bragg condition under multiple-scattering conditions. An independent measurement of the incident-beam intensity is needed for every thickness. The variation of crystal thickness allowable between different orientations should be small on the scale of the smallest $L^{(j)}$, so that atomically smooth surfaces are not required.

It is possible that by suitable choice of the illumination aperture shape it may be possible to excite several different independent pairs of diffraction patterns (with interference occurring only within each pair), so that more than one pair of columns in $\mathbf{S}$ might be phased for each probe scan. This process is limited by the range of coherence across the aperture, and by the need to avoid allowing three incident beams to contribute to each measured intensity.

We note that the nonrelativistic dynamical theory contains only products of the electron wavelength and the crystal thickness. This may be most useful in dealing with degenerate eigenvalues and/or near thicknesses where the ordering of eigenvalues changes abruptly. (At relativistic energies, the diagonal and off-diagonal elements of $\mathbf{A}$ have different dependencies on electron wavelength.)

The Bravais lattice and cell constants may be determined with an accuracy of about one part in 10^{-4}, using the novel technique of Zuo (1994), which is based on measurements of the positions of the fine three-dimensional HOLZ lines in the central convergent-beam

disc. Taken together, these two methods may therefore provide a general method for solving unknown micro-crystal structures by electron diffraction.

APPENDIX A
A f.c.c. (111) zone-axis pattern

In order to clarify the method for the purposes of algorithm development, the indexing of the scattering matrix is given below for a face-centered cubic structure in the (110) zone-axis orientation, with seven beams forming a two-dimensional pattern. The central column $C4$ contains quantities whose squared moduli are the multiply scattered Bragg-beam intensities for the upper indexed reflection. These are the beams in the experimental pattern selected for analysis. It can be seen that the entire matrix can then be indexed from a knowledge of $C4$.

$$S(\mathbf{K}_t = 0) = \begin{array}{ccccccc}
C1 & C2 & C3 & C4 & C5 & C6 & C7 \\
00\bar{2}/00\bar{2} & 00\bar{2}/1\bar{1}\bar{1} & 00\bar{2}/1\bar{1}1 & 00\bar{2}/000 & 00\bar{2}/\bar{1}1\bar{1} & 00\bar{2}/\bar{1}11 & 00\bar{2}/002 \\
1\bar{1}\bar{1}/00\bar{2} & 1\bar{1}\bar{1}/1\bar{1}\bar{1} & 1\bar{1}\bar{1}/1\bar{1}1 & 1\bar{1}\bar{1}/000 & 1\bar{1}\bar{1}/\bar{1}1\bar{1} & 1\bar{1}\bar{1}/\bar{1}11 & 1\bar{1}\bar{1}/002 \\
1\bar{1}1/00\bar{2} & 1\bar{1}1/1\bar{1}\bar{1} & 1\bar{1}1/1\bar{1}1 & 1\bar{1}1/000 & 1\bar{1}1/\bar{1}1\bar{1} & 1\bar{1}1/\bar{1}11 & 1\bar{1}1/002 \\
000/00\bar{2} & 000/1\bar{1}\bar{1} & 000/1\bar{1}1 & 000/000 & 000/\bar{1}1\bar{1} & 000/\bar{1}11 & 000/002 \\
\bar{1}1\bar{1}/00\bar{2} & \bar{1}1\bar{1}/1\bar{1}\bar{1} & \bar{1}1\bar{1}/1\bar{1}1 & \bar{1}1\bar{1}/000 & \bar{1}1\bar{1}/\bar{1}1\bar{1} & \bar{1}1\bar{1}/\bar{1}11 & \bar{1}1\bar{1}/002 \\
\bar{1}11/00\bar{2} & \bar{1}11/1\bar{1}\bar{1} & \bar{1}11/1\bar{1}1 & \bar{1}11/000 & \bar{1}11/\bar{1}1\bar{1} & \bar{1}11/\bar{1}11 & \bar{1}11/002 \\
002/00\bar{2} & 002/1\bar{1}\bar{1} & 002/1\bar{1}1 & 002/000 & 002/\bar{1}1\bar{1} & 002/\bar{1}11 & 002/002
\end{array}$$

In this matrix, according to (7), the symbol $00\bar{2}/\bar{1}11$ for example means

$$C_{g,h} = \sum_{i=1}^{7} C_{00\bar{2}}^{(i)} C_{\bar{1}11}^{(i)} \exp(2\pi\gamma^{(i)}t).$$

From this scattering matrix, the structure matrix **A** may be indexed in a manner consistent with the dispersion equation (4) as follows, using the central column of **S** to index the diagonal of **A**:

$$\mathbf{A} = \begin{array}{ccccccc}
00\bar{2} & \bar{1}1\bar{1} & \bar{1}1\bar{3} & 00\bar{2} & \bar{1}1\bar{1} & \bar{1}1\bar{3} & 00\bar{4} \\
1\bar{1}1 & 1\bar{1}\bar{1} & 002 & 1\bar{1}\bar{1} & \bar{2}20 & \bar{2}2\bar{2} & 1\bar{1}\bar{3} \\
1\bar{1}3 & 00\bar{2} & 1\bar{1}1 & 1\bar{1}1 & \bar{2}2\bar{2} & \bar{2}20 & 1\bar{1}\bar{1} \\
002 & \bar{1}11 & \bar{1}1\bar{1} & 000 & 1\bar{1}\bar{1} & 1\bar{1}1 & 00\bar{2} \\
\bar{1}11 & \bar{2}20 & \bar{2}2\bar{2} & 1\bar{1}\bar{1} & 1\bar{1}\bar{1} & 00\bar{2} & 1\bar{1}\bar{3} \\
\bar{1}1\bar{3} & \bar{2}2\bar{2} & \bar{2}20 & \bar{1}11 & 002 & \bar{1}1\bar{1} & \bar{1}1\bar{1} \\
004 & \bar{1}13 & 111 & 002 & 1\bar{1}3 & 1\bar{1}\bar{1} & 002
\end{array}.$$

Here the diagonal elements are the indices of the excitation errors, while off-diagonal elements are quantities $U_{g-h}/2K$, as in equation (5). The inversion will generate this matrix of structure factors.

We consider now the experiments needed to find all the phase differences between columns 5 and 6 of **S** as an example. The geometry of the diffraction pattern is given in Fig. 6.

Shown in Fig. 7 are the two Laue-circle constructions required to find these phase differences, using $\mathbf{K}_t^{(1)} =$

$(\bar{1}1\bar{1})$ and $\mathbf{K}_t^{(2)} = (\bar{1}11)$ since these are the unchanging indices of $C5$ and $C6$. The Laue circle is the intersection of the Ewald sphere with the ZOLZ. Unlike this reciprocal-space diagram, the experimental diffraction patterns do not share a common origin and consist of two spot patterns (one for each $\mathbf{K}_t$ value) with a relative displacement of (002) superimposed. This choice of orientations may be justified by working back from the matrix $\mathbf{S}(\mathbf{K}_t = 0)$ to the experimental arrangement. From the matrix, interference between columns five and six would result from terms of the form

$$\phi = \sum_{i=1}^{7} C_{\mathbf{g}}^{(i)}(0) C_{\bar{1}1\bar{1}}^{(i)}(0) \exp(2\pi\gamma^{(i)}t)$$

$$+ \sum_{i=1}^{7} C_{\mathbf{g}}^{(i)}(0) C_{\bar{1}11}^{(i)}(0) \exp(2\pi\gamma^{(i)}t).$$

Using the periodicity relations equations (11) and (10) [with $\mathbf{k}^{(i)}(x, y) = 0$] and using $\mathbf{K}_t^{(1)} = -\mathbf{h} = (\bar{1}1\bar{1})$ and $\mathbf{K}_t^{(2)} = -\mathbf{h}' = (\bar{1}11)$, this becomes

$$\phi = \sum_{i=1}^{7} C_{\mathbf{g}-\bar{1}1\bar{1}}^{(i)}(\bar{1}1\bar{1}) C_0^{(i)}(\bar{1}1\bar{1}) \exp[2\pi(\gamma_{\bar{1}1\bar{1}}^{(i)} - s_{\bar{1}1\bar{1}})t]$$

$$+ \sum_{i=1}^{7} C_{\mathbf{g}-\bar{1}11}^{(i)}(\bar{1}11) C_0^{(i)}(\bar{1}11) \exp[2\pi(\gamma_{\bar{1}11}^{(i)} - s_{\bar{1}11})t]$$

$$= \Phi_{\mathbf{g}-\bar{1}1\bar{1}}(\bar{1}1\bar{1}) \exp(2\pi s_{\bar{1}1\bar{1}}t)$$

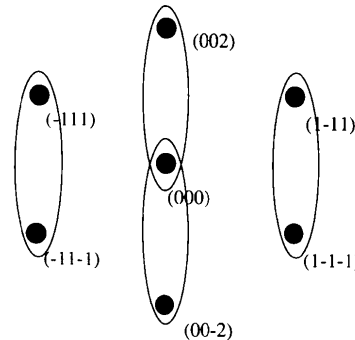$$+ \Phi_{\mathbf{g}-\bar{1}11}(\bar{1}11) \exp(2\pi s_{\bar{1}11}t),$$

Fig. 6. Diffraction pattern from a f.c.c. crystal in (110) orientation formed with an elliptical illumination aperture.
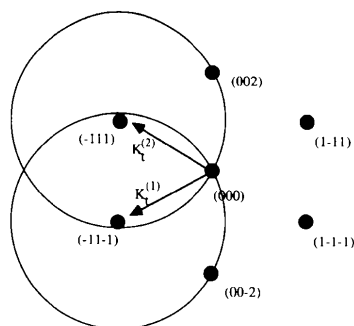
Fig. 7. Laue-circle constructions for the two incident-beam directions needed to 'interfere' columns 5 and 6 of the scattering matrix for Fig. 5. Values of K_t are given by the unchanging index of these columns.

where the indexed arguments in parentheses are the values of K_t. Apart from the phase factors involving excitation errors (which are known), this equation describes the experimental arrangements shown above – two patterns with different K_t values (the crystal tilt), superimposed after a displacement of (002), equal to the difference between the Φ subscripts.

Note added in proof: Orthogonality constraints aid the solution of equations (20).

References

Allen, L. & Rossouw, C. (1993). *Ultramicroscopy*, **48**, 241–248.

Bethe, H. A. (1929). *Ann. Phys. (Leipzig)*, **87**, 55–128.

Bird, D. (1990). *Acta Cryst.* A46, 208–214.

Blackman, M. (1939). *Proc. R. Soc. London Ser. A*, **173**, 68–82.

Cantoni, A. & Butler, P. (1976). *Linear Algebra and its Applications*, Vol. 13, pp. 275–288. New York: McGraw-Hill.

Cowley, J. M. (1978). *Inst. Phys. Conf. Ser.* No. 41, pp. 156–166.

Cowley, J. M. (1986). *J. Electron Microsc. Tech.* **3**, 25–38.

Cowley, J. M. (1992). *Techniques of Transmission Electron Diffraction.* New York: Oxford University Press.

Dorset, D. L. (1995). *Structural Electron Crystallography.* New York: Plenum.

Gjønnes, J. & Høier, R. (1971). *Acta Cryst.* A27, 313–316.

Hirsch, P. S., Howie, A., Nicholson, R. B., Pashley, D. W. & Whelan, M. J. (1977). *Electron Microscopy of Thin Crystals.* New York: Robert E. Krieger.

Høier, R. (1972). *Phys. Status Solidi A*, **11**, 597–601.

Humphreys, C. J. (1979). *Rep. Prog. Phys.* **42**, 1825–1868.

Kambe, K. (1957). *J. Phys. Soc. Jpn*, **12**, 13–26.

McCallum, B. C. & Rodenberg, J. M. (1992). *Ultramicroscopy*, **45**, 371–388.

Metherell, A. J. F. & Fisher, R. M. (1969). *Phys. Status Solidi*, **32**, 551–563.

Moodie, A. F., Etheridge, J. & Humphreys, C. J. (1996). *Acta Cryst.* A52, 596–605.

Moodie, A. F. & Whitfield, H. (1994). *Acta Cryst.* A50, 730–736.

Nellist, P. D., McCallum, B. & Rodenberg, J. (1995). *Nature (London)*, **374**, 630–632.

Nellist, P. D. & Rodenberg, J. M. (1994). *Ultramicroscopy*, **54**, 61–64.

Niehrs, H. (1959). *Z. Naturforsch. Teil A*, **14**, 504–515.

Rez, P. (1978). *Acta Cryst.* A34, 48–51.

Rez, P. (1979). *Phys. Status Solidi A*, **55**, K79–81.

Saldin, D. & Spence, J. (1994). *Ultramicroscopy*, **55**, 397–406.

Scheerschmidt, K. & Knoll, F. (1995). *Electron Holography*, edited by A. Tonomura, L. Allard, G. Pozzi, D. Joy & Y. Ono, pp. 117–124. New York: Elsevier.

Smith, B. T. (1976). *Lecture Notes in Computer Science.* Berlin: Springer-Verlag.

Spargo, A., Beeching, M. & Allen, L. J. (1994). *Ultramicroscopy*, **55**, 329–338.

Speer, S., Spence, J. C. H. & Ihrig, E. (1990). *Acta Cryst.* A46, 763–772.

Spence, J. (1978). *Scanning Electron Microscopy*, edited by O. Johari, pp. 61–69. Chicago: IITRI.

Spence, J. C. H. (1988). *Experimental High Resolution Electron Microscopy.* New York: Oxford University Press.

Spence, J. C. H. & Cowley, J. M. (1978). *Optik (Stuttgart)*, **50**, 129–143.

Spence, J. C. H. & Zuo, J. M. (1992). *Electron Microdiffraction.* New York: Plenum.

Sturkey, L. (1962). *Proc. Phys. Soc. London*, **80**, 321–354.

Tanaka, M., Terauchi, M. & Tsuda, K. (1994). *Convergent Beam Electron Diffraction III*, pp. 223–224. Tokyo: Jeol-Maruzen.

Uyeda, R. (1968). *Acta Cryst.* A24, 175–181.

Vincent, R., Bird, D. M. & Steeds, J. W. (1984). *Philos. Mag.* A50, 765–784.

Vincent, R., Vine, W., Midgley, P. A., Spellward, P. & Steeds, J. (1992). *Ultramicroscopy*, **50**, 365–370.

Zuo, J. M. (1994). *Ultramicroscopy*, **52**, 459–470.

Zuo, J. M. & Spence, J. C. H. (1993). *Philos. Mag.* **68**, 1055–1073.

Zuo, J. M., Spence, J. C. H., Downs, J. & Mayer, J. (1993). *Acta Cryst.* A49, 422–429.